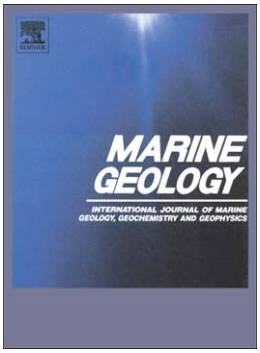

Chronology of the Fram Slide Complex offshore NW Svalbard and its implications for local and regional slope stability

Judith Elger, Christian Berndt, Sebastian Krastel, David J.W. Piper, Felix Gross, Wolfram H. Geissler

PII: S0025-3227(16)30302-4
DOI: doi:10.1016/j.margeo.2016.11.003
Reference: MARGO 5539

To appear in: *Marine Geology*

Received date: 29 January 2016
Revised date: 25 October 2016
Accepted date: 16 November 2016

Please cite this article as: Elger, Judith, Berndt, Christian, Krastel, Sebastian, Piper, David J.W., Gross, Felix, Geissler, Wolfram H., Chronology of the Fram Slide Complex offshore NW Svalbard and its implications for local and regional slope stability, *Marine Geology* (2016), doi:10.1016/j.margeo.2016.11.003

Chronology of the Fram Slide Complex offshore NW Svalbard and its implications for local and regional slope stability

Judith Elger [1, 2)], Christian Berndt [1)], Sebastian Krastel [2)], David J.W. Piper [3)], Felix Gross [2)], Wolfram H. Geissler [4)]

Corresponding author: Judith Elger, jelger@geomar.de

1) GEOMAR Helmholtz Centre for Ocean Research Kiel, Germany

2) Institut für Geowissenschaften, Christian-Albrechts-Universität zu Kiel, Germany

3) Geological Survey of Canada, Bedford Institute of Oceanography, Dartmouth, NS, Canada

4) Alfred-Wegener-Institut Helmholtz-Zentrum für Polar- und Meeresforschung, Bremerhaven, Germany

Abstract

The best known submarine landslides on the glaciated NW European continental margins are those at the front of cross-shelf troughs, where the alternation of rapidly deposited glycogenic and hemi pelagic material generates sedimentary overpressure. Here, we investigate landslides in two areas built of contourite drifts bounded seaward by a ridge-transform junction. Seismic and bathymetric data from the Fram Slide Complex are compared with the tectonically similar Vastness area ~120 km to the south, to analyze the influence of local and regional processes on slope stability. These processes include tectonic activity, changes of climate and oceanography, gas hydrates and fluid migration systems, slope gradient, toe erosion and style of contourite deposition. Two areas within the Fram Slide Complex underwent different phases of slope failures, whereas there is no evidence at all for major slope failures in the Vastness area. The comparison cannot reveal the distinct reason for slope failure but demonstrates the strong impact of variation in the local controls on slope stability. The different failure chronologies suggest that toe erosion, which is dependent on the throw of normal faults, and the different thickness and geometry of contourite deposits can result in a critical slope morphology and exert pronounced effects on slope stability. These results highlight the limitations of regional hazard assessments and the need for multi-disciplinary investigations, as small differences in local controlling factors led to substantially different slope failure histories.

Keywords

Fram Strait; Svalbard continental margin; submarine landslides; slope stability; pre-conditioning; trigger mechanisms; gas hydrates

Highlights

- The Fram Slide Complex has been active from late Miocene to late Pleistocene.
- Local processes were critical for slope stability in the Fram Strait area.
- Toe erosion caused by normal faulting may have led to retrogressive failure.
- Low gradient contourite drifts might smooth and stabilize submarine slopes.
- Low tsunami potential from the Fram Slide Complex could increase in the future.

1. Introduction

Submarine slope failures are a worldwide phenomenon and represent a significant natural hazard. They can destroy offshore infrastructure and generate destructive tsunamis which endanger coastal communities. Numerous studies show that submarine landslides occurred in the Holocene and Pleistocene on the NE Atlantic glaciated margin (Fig. 1A) and concluded that the cyclic sedimentation pattern related to glacial/interglacial conditions critically influences slope stability (Laberg and Vorren, 2000; Haflidason et al., 2004; Lindberg et al., 2004; Hjelstuen et al., 2007; Winkelmann and Stein, 2007). This hypothesis fits well for slopes with failures at former maximum ice margins where the deposition of trough mouth fans led to very high sedimentation rates during glacial melting, presumed to lead to overpressure build-up in the sediment pore space. It does not explain the occurrence of submarine slope failures in other geological settings.

Future climate models predict that the Arctic will be mostly free of summer sea ice by the end of the 21st century (Stocker et al., 2013) and forecast a long-lasting bottom water warming. This trend may have an effect on gas hydrate stability while at the same time enhances the interest of the hydrocarbon industry to extend oil and gas exploration further north. Hence, it is necessary to improve our knowledge about the processes and settings that favour slope instability in order to assess hazards in the Arctic and to minimize the impact of seafloor stability on hydrocarbon exploitation.

There are not many submarine landslides known and studied in the European Arctic apart from the Hinlopen/Yermak slide complex (Winkelmann and Stein, 2007) and the Fram Slide (Elger et al., 2015). Elger et al. (2015) reported on the extent of the Fram Slide and compared it with the typical characteristics of slope failures on the NE Atlantic glaciated margin. That study confirmed that submarine slope failure in the NE

Atlantic is not restricted to areas close to the maximum ice extent. Rather, the Fram Slide Complex (FSC) is developed in a contourite drift, near the tectonically active intersection of the Spitsbergen Transform Fault and the Molløy Ridge (Fig. 1B). An analogous tectonic setting is found 120 km southeast, in the Vestnesa area on the Svalbard continental margin, in contourite drifts near the intersection of the Knipovich Ridge and the Molløy Transform Fault. No submarine landslides have been reported there previously.

The purpose of this paper is to constrain the chronology of events that shaped the Fram Slide Complex (FSC) based on a new seismic and bathymetric data set. A second objective is to evaluate the role of regional and local geological processes that pre-condition and trigger submarine landslides, by comparing the internal variability in morphology and recurrence interval of landslides in the FSC and the Vestnesa area. Tectonic activity, influence of climate and oceanography, and contourite deposition are considered processes that shape the slope and can lead to toe erosion and over-steepening, whereas gas hydrates and basinal fluids are relevant for buoyancy-related overpressure. In addition, we assess the hazard of the FSC by comparing its features with other slope failures on the eastern glaciated North Atlantic continental margin and their estimated hazard.

2. Regional setting

The FSC is located at the intersection of the Spitsbergen Transform Fault and the Molløy Ridge in the Fram Strait that connects the Eurasian Basin with the Norwegian and Greenland Sea (Fig. 1A). When the Eurasian and North American plates separated in the earliest Eocene, the two basins were connected by a strike-slip fault. From the earliest Oligocene, motion between Greenland and Eurasia changed from transform to divergent and the sheared margin was rifted and broken into ridges connected by transform faults (Talwani and Eldholm, 1977). The Spitsbergen Transform Fault is the most prominent of several transform faults that connect the

adjacent spreading ridges and move in a dextral shear sense (Engen et al., 2003) (Fig. 1B). It forms a narrow northwest–southeast oriented valley with a length of ~150 km connecting the southern Lena Trough in the north with the 60-km-long Molløy Ridge in the south. The Molløy Ridge is bounded to the southeast by the Molløy Transform Fault, which intersects with the Knipovich Ridge in the Vestnesa area.

Present day oceanographic conditions are characterized by the northward inflow of the West Spitsbergen Current carrying warm Atlantic Water into the Arctic Ocean (Manley, 1995) (Fig. 1A). At ~79.0°N the West Spitsbergen Current splits into three branches (Quadfasel et al., 1987) (Fig. 1B). The Svalbard Branch turns eastward directly north of the Svalbard archipelago and flows across the shallow southern Yermak Plateau (Schauer et al., 2004). The west branch flows southwards and joins the East Greenland Current (Bourke et al., 1988) and the Yermak Plateau Branch transports water northwards along the western Yermak Plateau where it enters the Arctic Ocean (Rudels et al., 2002).

An initial oceanic channel connected the Eurasian Basin with the Norwegian-Greenland Sea since earliest Miocene (Thiede et al., 1995) but the present day mode of seafloor spreading was probably delayed until late Miocene (Engen et al., 2008). A major provenance change of sediments at 11.2 Ma documented in sediment cores of ODP Leg 151 (Winkler et al., 2002) supports this tectonic change. The connection of the two basins led to gradual cooling of the northern hemisphere, as evidenced by ice-rafting activity from 5.7 to 3.2 Ma (Wolf and Thiede, 1991). Long-lasting moderate glacial conditions from 2.6 to 1.0 Ma were followed by increased glacial/interglacial environmental conditions until 0.6 Ma. These climate conditions were associated with the transition to characteristic glacial and interglacial shifts in deep water properties. From 0.6 Ma to present, large differences in glacial/interglacial environmental conditions with a maximum contrast in surface water regimes led to different modes of deep water production and exchange rates with the North Atlantic (Henrich and Baumann, 1994; Henrich, 1998).

In both the FSC and the Vestnesa area, plastered sediment drifts with large-scale sediment waves have developed on the Svalbard continental margin. The Vestnesa Ridge, a NW-SE elongated sediment drift north of the Molløy Transform Fault, indicates the great influence of contour currents in the Vestnesa area that led to high sedimentation rates. Gas hydrate and free gas within the drift form gas seeps and have been subject of several studies (Hustoft et al., 2009; Petersen et al., 2010).

3. Materials and methods

This study uses multibeam data from the FSC and Vestnesa area that were acquired during cruises MSM31 (FSC only) and MSM21/4 with the hull-mounted Kongsberg EM122 and EM120 system, respectively (Figs. 2A, 3A). Both systems operate with an angular coverage of 150° and a nominal transducer frequency of 12 kHz. We used the open source MB System software for processing, GMT for gridding at various bin sizes and ArcGIS for the calculation of slope angles. The illustrated grids have a horizontal bin size of 50 m.

2D high-resolution reflection seismic data acquired during cruises MSM21-4 and MSM31 cross the slope in different parts of the FSC (location in Fig. 2A, coordinates in the supplementary material Table S1). Seismic data were collected with an 88-channel Geometrics GeoEel streamer of a total length of 137.5 m and a group spacing of 1.5625 m. The signal was generated by a 1.7 l GI-Gun, shot at 200 bar at ~2 m tow depth. We used the VISTA package (Schlumberger) for seismic processing. Data were binned at 3.125 m. Normal move out correction was carried out with a constant velocity of 1500 m/s and an Ormsby band pass filter with corner frequencies at 40, 80, 600 and 1000 Hz was applied. Finite difference time migration was performed with a constant velocity of 1500 m/s. A shot interval of 7 s and a recording length of 6 s were chosen at a cruise speed of ~ 4.5 knots to obtain an average CMP (Common-Mid-Point) fold of ~15 by applying a bin size of 3.125 m. The wavelet of the reflections in the water column shows peak energy at frequency ~100 Hz. Assuming a

constant sound speed of 1500 m/s, the vertical resolution is ~3.75 m. Seismic data from the Vestnesa area were filtered in the shot gather domain by a τ-p filter to suppress surface-generated water noise. A zero-phase band-pass filter was applied, using corner frequencies of 60 Hz and 360 Hz. For normal move out correction an interpolated and extrapolated 3D velocity model based on regional velocity information from multichannel seismic data (Sarkar et al., 2012) was used. Common midpoint (CMP) profiles were generated through crooked-line binning with a CMP spacing of 1.5625 before applying an amplitude preserving Kirchhoff post-stack time migration (Dumke et al., 2016).

In order to estimate the minimal age of the landsliding, we applied the seismic stratigraphy from Mattingsdal et al. (2014). Mattingsdal et al. (2014) used paleomagnetic and biostratigraphic samples in combination with high-resolution seismic data connecting ODP holes to establish a comprehensive stratigraphic framework for the Fram Strait for the last 6 Ma (location in Fig. 2A). Although our seismic profiles do not intersect the lines used for that stratigraphy (Fig. 1B), typical reflection patterns in the seismic profiles of undisturbed sediments at the top of the slope were correlated confidently and allow ages to be assigned to particular seismic horizons. We estimate the uncertainty for the ages of old slope failures (~5 Ma) to be on the order of 1 Ma, and for the recent slope failures to be on the order of 100 ka. Headwalls and sidewalls that occur at the same stratigraphic level and are connected by one surface expression in the bathymetry were combined to one slope failure. We calculated the maximum evacuated volume of the failures by multiplying the affected area derived from the bathymetry (from the headwall down to the slope break in ~3 km water depth) with the maximum height of the headwall. This approach to volume estimation contains large uncertainty but it is the best procedure possible considering the data base.

4. Results

4.1. Seafloor morphology of the FSC

Based on new bathymetric data, the FSC covers an area of 5500 km² east of the Spitsbergen Transform Fault in water depths between 850 m to 4200 m (Figs. 1B and 2A). This is more than twice the area previously estimated (Elger et al., 2015). The gradient map in Fig. 2B shows that the slope is divided into areas of maximal 2.7 ° dip mostly at the top of the slope, minor steep parts (3 to 8°) in the upper part of the slope and very steep parts of up to 22° at the very bottom of the slope. In the northern part, the minor steep slope (3 to 8 °) is up to 25 km distant from the surface expression of the Spitsbergen Transform Fault, separated by a gently sloping area (< 2.7°). In the southern part of the FSC, a narrow stretch of margin of only 10 km links the upper part of the slope with the depression of the Molløy Ridge and Spitsbergen Transform Fault (Fig. 2B). The bathymetric and gradient maps show a large number of morphological steps on the upper part of the slope that illustrate the characteristic amphitheatric shape of headwalls and sidewalls of submarine landslides (Figs. 2A and 2B).

North of 79°55'N (northern part of the FSC), a displacement of up to 270 m height and 100 km length is the most prominent morphological feature of the seafloor (Fig. 2A). Seismic data show a buried scarp that truncates in total ~600 m thick, well stratified sediments (Fig. 4). Hence, this structure originates from a buried, large-scale slope failure with different glide planes in the very northern part of the FSC. This interpretation is similar to the composite set of escarpments and multiple buried slip surfaces of the Hinlopen Yermak slide with its >1000 m high headwall (Vanneste et al., 2006). Other minor scarps on the seafloor close to the buried large-scale headwall (Figs. 2A and 2B) are identified as buried headwalls based on seismic interpretation (Fig. 4).

Numerous smooth and sharp steps of heights from 30 to 200 m on the seafloor (Fig. 2A) characterize the morphology south of 79°55'N (southern part of the FSC). The seismic data do not cover the entire area but reveal a minimum of 16 headwalls of heights of up to 120 m that are covered by sediments of different thickness (Fig. 5). The seafloor morphology of this part of the slide complex is not dominated by one structure but consists of a variety of diverse headwalls (compare Figs. 2A and 2B).

4.2. Chronology and volume of failures of the FSC

The slope failures that caused the headwalls occurred before 5 Ma to about 0.68 Ma applying the seismic stratigraphy from Mattingsdal et al. (2014) (Table 1 and Fig. 6). Before 5 Ma a submarine slope failure formed major headwalls and sidewalls in the northern part and evacuated ~1160 km³ of sediment. Minor slope failures in the vicinity of this structure created scarps of 23 to105 m height and occurred less than 2.58 to 0.78 Ma ago (Table 1 and Fig. 6). Heights of the headwalls and corresponding volumes decrease over time, with the smallest features being the youngest. The chronology of the events in the southern part of the FSC shows a much more even distribution of slope failures in the time period of >5 to 0.68 Ma (Table 1 and Fig. 6). There is no distinct correlation between age, water depth or height of the headwalls. The estimated volumes of failed sediment range from 3 to 62 km³. The slope failures that caused maximum headwall heights of 120 m originated at about 0.78 Ma (Table 1).

4.3. Subsurface features of the FSC

Seismic data image a series of seismic high-amplitude anomalies running parallel to the seafloor. They cut the sediment layers at ~300 ms two-way travel time (twtt) or ~225 m below the sea floor (assuming a sediment sound velocity of 1500 m s^{-1}). The anomalies terminate in this depth and in some places (e.g. Fig. 5) they form a continuous seismic reflection. We interpret these anomalies as a bottom simulating reflection (BSR), similar to those observed elsewhere along the Svalbard and mid-Norwegian margin (Berndt et al., 2004). The BSR marks the base of the gas hydrate stability zone. Free gas accumulating underneath the gas hydrate stability zone appears as areas of enhanced negative phase amplitudes.

Generally, we identify a coherent BSR in the upper part of the slope but further downslope there are only local high-amplitude reflections at the expected depth of the BSR. Shedd et al. (2009) termed such a series of bright spots a 'segmented' BSR. The two southern seismic profiles (Fig. 2A) image the BSR well on the entire slope down to 2900 m water depth (Fig. 5). At the sidewall in the northern part of the FSC, the BSR is visible from the top down to the bottom of the sidewall (Fig. 4). It cuts the stratigraphy of the pre-failure sediments but not the sediments that accumulated afterwards. Gas is trapped underneath the uppermost layer that did not fail. This phenomenon appears at several locations and may represent sealing sediments that trap gas and may create buoyancy-related overpressure.

Several steeply dipping low-amplitude anomalies interrupt seismic reflections of layered sediments with changing dip (Fig. 7) in the southern part of the complex and correspond to bathymetric escarpments (Fig. 2A). As they are associated with rotational downward displacement of the seismic reflections, we interpret them as normal faults of up to 120 m throw (average 41 m, using a velocity of 1500 ms^{-1}). There are three types of

faults. Faults with a curved trace follow the shape of the deep water pathway built by the depressions of the Molløy Ridge and Spitsbergen Transform Fault and terminate at the slope in ~3 km water depth. Further upslope, in the lower part of the slide area (2300-3000 m water depth), faults with a strike direction of ~055° dip towards the southwest. Another set of faults strikes ~010° and dips south-southwest (Fig. 2A).

Seismic data in the southern part of the FSC image lateral thickness variations of reflection packages as well as unconformities that form wavy layers (Fig. 8). These characteristics indicate current-controlled deposition which we interpret as sediments waves, discordances and moats. These sediment structures document the spatial and temporal variation of contour currents in water depths between 1700 and 2800 m and their influence on the sedimentation process on the slope.

4.4 Characteristics of the Vestnesa area

Based on bathymetric data (Fig. 3A), the slope in the Vestnesa area (Fig. 3B) is divided into a region with a maximum gradient of 2.7° at the top of the slope, minor steep parts (2.7 to 11°) and a steep region with gradients of up to 20° at the bottom of the slope. The bathymetric map shows a few morphological steps (Fig. 3A) but the seismic data illustrate no evidence for buried or recent major slope failures at a scale clearly resolved in seismic data (Fig. 9). It reveals high-amplitude anomalies parallel to the seafloor that transect through sediment layers at ~250 ms twtt beneath the sea floor reflection (Fig. 9). This ‘segmented’ BSR (cf. Shedd et al., 2009) marks the base of the gas hydrate stability zone and implies free gas underneath (Vanneste et al., 2005). This interpretation corresponds to several studies that showed active gas venting in the gas hydrate system in this region (e.g. Hustoft et al., 2009). The seismic data also show normal faulting (Fig. 9) with throws of up to 37 m (average 12 m). The lateral thickness of the sediments is mostly constant. Only on the very

eastern profiles lateral thickness variations and wave-like patterns clearly indicate current controlled deposition (Fig. 9).

5. Discussion

5.1. Timing and evolution of the Fram Slide Complex

The entire FSC has been active from the late Miocene until the late Pleistocene (at least 60 ka BP (Elger et al., 2015)) (Fig. 6 and Table 1). Slope failures in the FSC occurred since the formation of the present day configuration of the Fram Strait as an oceanic gateway (Engen et al., 2008). There is no obvious limitation or concentration of events to a certain period regarding the entire area of the FSC. Therefore, the FSC stands out from most other studied large-scale slope failures on the glaciated Northeast Atlantic margin which are primarily dated to the Holocene and Pleistocene (Hjelstuen et al., 2007). On the other hand, it resembles the pattern of slope failures known from the lower latitude glaciated margin off Nova Scotia (Campbell et al., 2004), in the Northwest Atlantic.

A detailed spatial analysis of slope failures (Fig. 6) shows that the northern part of the FSC is primarily shaped by one major slope failure that occurred more than 5 Ma ago (slope failure N0 in Table 1). It stands out from all other events because the headwall is overall ~600 m high and the calculated volume of failed material (~1160 km^3) is about 60 times larger than of most of the other failures. Sediments that deposited before this slope failure are horizontally layered and there is no evidence in the seismic data that they are underlain by an older headwall (Fig. 4). These characteristics suggest that it is the initial slope failure in the northern part of the FSC.

Younger and much smaller slope failures in that area seem to be related to over-steepening, as they are restricted to the vicinity of this old headwall (Figs. 2A and 4). The history of slope failures in the southern part of the FSC started in the late Miocene, approximately at the same time as in the northern part, but involving smaller volumes (2-3% of the volume that failed during N0) (Table 1). Since this time, the reflection seismic data document repeated slope failures until the late Pleistocene, with volumes of 2 to 62 km³ along the entire slope between 1290 and 2440 m water depth (Fig. 6). Thus, slope failure evolution in the northern part and the southern part of the FSC clearly differ in size, age and recurrence interval.

5.2. Regional controlling mechanisms

Most slope failures in the North Atlantic on the European margin are located directly at or down-current from trough mouth fans or ice stream outlets (Fig. 1A). This fact led to the conclusion that the main driving processes which decrease slope stability on the glaciated North Atlantic margin are related to glacial sediment deposition and seismicity due to rapid glacial unloading caused by the glacial cycles (Bryn et al., 2005; Kvalstad et al., 2005; Leynaud et al., 2009; Piper et al., 2012). Build-up of extensive overpressure reduces the effective stress and makes slopes prone to slope failure, especially if they contain particularly unstable hemipelagic layers. A trigger, e.g. an earthquake, can activate a preconditioned system through a further increase of pore pressure or deformation of sediments and lead to liquefaction. The location of the FSC in a more distal setting relative to proximal plume deposits, ~35 km to the Sjubrebanken trough mouth fan and ~85 km down-current from of the Kongsfjorden cross-shelf trough (Fig. 1B), does not match such typical characteristics. Its location indicates that there are probably different processes that are critical for slope stability in distal settings. For example, on the glaciated Scotian margin distant from trough-mouth fans, Mosher et al. (2004) suggested processes such as salt tectonics, erosional over-steepening in canyons by turbidity currents, lateral spreading failure (creep), and the influence on pore pressure of hydrocarbon gas or

other deep-seated fluid seepage all preconditioned glacial plume deposits for failure. In order to identify regional processes that were important for the slope stability in the Fram Strait, we concentrate on the significantly different evolution of slope failure history in the northern and southern part of the FSC. We compare them with the Vestnesa area (Fig. 1), where previous studies (Sarkar et al., 2012; Plaza-Faverola et al., 2015) and our seismic interpretation show no evidence for major slope failures in the seismically imaged section.

5.2.1. Tectonics

The history of slope failures in the FSC is restricted to the time when the region was tectonically active with the present day mode of seafloor spreading (Engen et al., 2008). Previous studies identified the seismicity and steep slopes linked the fault and ridge systems as destabilization factors that potentially represent an environment vulnerable to slope failure (Schwab et al., 1991, Gardner et al., 1999). The magnetic anomalies identified by Engen et al. (2008) suggest comparable spreading rates in the Fram Strait and the Vestnesa area and indicate a similar history of seismicity. Recent seismicity along the transform faults and the ridges is documented by the United States Geological Survey (1973-2015) and show no obvious difference regarding either recurrence frequency or magnitude (Fig. 1B). Based on available data we interpret all three locations to be equally influenced by large-scale tectonic activity and earthquakes that may serve as a trigger mechanism for submarine landslides. The tectonic setting does not explain the local differences in slope stability and failure recurrence frequency.

5.2.2. Climate and Oceanography

At the beginning of the slope failure history of the FSC in the late Miocene, the climate and oceanographic setting of the region was predominantly linked to the opening of the Fram Strait. Equal spreading rates in the FSC and Vestnesa area (Engen et al., 2008) indicate that regional changes of climate and oceanographic conditions as well as the eustatic changes in sea level probably developed similarly along the entire area between the Lena Trough and the Knipovich Ridge. During the remaining development of the FSC, the cyclic changes due to glacial and interglacial conditions were the main influence on regional oceanographic characteristics. The resulting changes in deep water production, water temperature and current velocity (Henrich and Baumann, 1994; Henrich, 1998) likely had the same impact on the entire area. Isostatic sea level change due to the build-up of ice and the influence of post-glacial rebound might have had slightly different impact on the FSC and the Vestnesa area, as the latter is closer to the edge of the maximal ice extent during glacial periods of the last 100 ka (Fig. 1). These local effects do not appear to have been significant, as recent slope failures are absent in the Vestnesa area. They cannot explain the local differences in slope stability within the FSC.

5.2.3. Gas hydrates and fluid migration

The third regional process that could be considered to influence the slope stability in the three locations is the existence of gas hydrates and fluid migration. Seismic data show a BSR as an indicator for the presence of gas hydrates above free gas in the northern area of the FSC only, close to the ancient headwall (Fig. 4), but almost continuously in the southern part (Fig. 5).This spatial correlation could be biased by the limited data coverage (Fig. 2A). A BSR is also widespread in the Vestnesa area (Dumke et al., 2016) (Fig. 9).

Several studies have discussed the potential of gas hydrate dissociation due to changing temperate and pressure conditions to reduce slope stability (e.g. Sultan et al., 2004) but there is no clear evidence that this process is a main driver for slope failure. There have been periods of increased bottom water temperatures of up to 6°C in the past (Miocene Climate Optimum, ~17–15 Ma) (Zachos et al., 2001) in the Fram Strait that would have increased the minimum water depth of the gas hydrate stability zone. Today, this minimum water depth, 550 m in the Arctic and as little as 380 m off Norway according to Kretschmer et al. (2015), is much shallower than all three locations studied, which have water depths greater than 1300 m (Figs. 2A and 3A). Warming would rather slowly elevate the base of the gas hydrate stability zone by conductive heat transport at these water depths. Pressure conditions might have changed due to sea level rise, for example during the Paleocene-Eocene Thermal maximum (Harding et al. (2011). However, Hunter et al. (2013) showed that even rapid sea level change (> 15 mm yr^{-1}) cannot significantly counteract the thermal effects on gas hydrate stability, particularly at great water depth (Mienert et al., 2005). We conclude that the water depths of the three locations exclude gas hydrate dissociation as a direct driver for slope failures.

A relationship of the major slope failure in the northern part of the FSC to gas hydrate-related processes is particularly unlikely, as the sidewall is higher than the expected gas hydrate stability zone. For the southern part of the FSC and the Vestnesa area we cannot exclude that the presence of gas hydrates could influence slope stability as a result of fluid migration. The volume of free gas underneath the BSR probably varied temporally and may have led to buoyancy-related overpressures that may have destabilized the slopes. Fluid migration structures that are revealed in the seismic data in the southern area (Elger et al., 2015) and the active gas venting in the Vestnesa area (Bünz et al., 2012) could be indications for preconditioning due to elevated overpressures (Karstens and Berndt, 2015). In combination with an earthquake, this elevated pore pressure could drive failure on low-angle slopes (Stigall and Dugan, 2010).

5.3 Local controlling factors

We did not find any evidence that regional processes for the formation of potentially unstable sedimentary successions nor seismicity as trigger mechanisms can explain the different pattern of slope failures in the three regions. We conclude, therefore, that local processes are crucial factors for slope stability. In the following, we discuss (1) the slope gradient, (2) toe erosion induced by rotational slumps, and (3) the distribution and architecture of contourites as significant factors for the different pattern of slope failure in the Vestnesa area and the two parts of the FSC.

5.3.1 Slope gradient

The seafloor morphology in the three areas (Figs. 2A and 3A) is predominantly controlled by the tectonic setting of transform faults and slow spreading ridges (Fig. 1B), which are expressed on the seafloor as ~1 km deep depressions. The headwalls and sidewalls in the entire FSC are located in the upper part of the slope where the gradient ranges between 3 and 8° (Fig. 2B). In the Vestnesa area the gradient of the upper slope is 2.7 to 11° (Fig. 3B). Hühnerbach et al. (2004) showed that most source areas of slope failures in the eastern North Atlantic have gradients of 2–6°. Neither the value nor distinct regional differences of the gradient of the upper slope explain the different failure pattern in the three regions.

The lower part of the slopes is similarly steep in all three areas and reaches maximum gradients of 22° (Figs. 2B and 3B). The distinct difference consists in the connection of the upper and lower slope. In the northern area of the FSC, they are separated by up to 25 km and connected by a gently dipping area (gradient < 2.7°) (Fig.

2B). In the southern part of the FSC, a corresponding narrower stretch (~10 km) of low gradient slope (gradient ≤ 6°) separates the upper part of the slope from the depression of the Molløy Ridge and Spitsbergen Transform Fault (Fig. 2B). In the Vestnesa area, there is no break of slope and the seafloor dips almost continuously towards the Molløy Transform Fault (Fig. 3B).

The slope gradient does not seem to be a discrete reason for slope failure in the considered areas, neither in the upper slope where the headwalls are located nor in the lower part at the toe of the slope. Within the FSC, repeated slope failure occurs only where the upper and lower parts of the slope are connected by a narrow, mid-gradient slope. Here, the entire slope reaches the critical gradient for retrogressive failure of at least 2° as proposed by Hühnerbach et al. (2004). This observation indicates that over-steepening, especially due to toe erosion, potentially led to retrogressive slope failure in the FSC. The overall equally dipping steep slope in the Vestnesa area in combination with absence of evidence for slope failures support this hypothesis. Given that gradients at the top of the slope in all compared areas are nearly equal, we consider processes and structures at the toe of the slope to be the determining factor for the differences in slope stability.

5.3.2 Toe erosion

Seismic data in the southern part of the FSC reveal normal faults down to 250 m below sea floor at the top of the lower slope in ~3 km water depth (Fig. 7). Tectonically induced strike-slip faults would typically strike linear and parallel to the slope and the strike of the Spitsbergen Transform Fault (Reches, 1987). Due to the curved, amphitheater-like expression of the faults in the bathymetric data, we hypothesize that they are predominantly gravity faults with listric detachment planes that were induced by the gravitational stress next to the depression of the Spitsbergen Transform Fault and Molløy Ridge (Figs. 2A and 7). This interpretation

implies rotational block movements along the gravity faults, which potentially cause toe erosion and could have destabilized the slope from the bottom upwards and led to retrogressive slope failures in the upper part of the slope. This failure dynamics corresponds to the results of Elger et al. (2015) and could be the reason for repeated slope failure in the southern FSC documented by multiple normal faults (average offset of 41 m) and headwalls of different age (Fig. 5). However, seismic profiles do not cover the top of the lower slope in the northern part (Fig. 2A). Based on limited bathymetric data and the similar setting, we expect that normal faults formed there as well. The distance between the upper and lower slope of ~25 km on a gradient of ~2° would have prevented this process from affecting slope stability in the northern part of the FSC.

The equally dipping slope in the Vestnesa area is also characterized by a steep lower slope (Fig. 3B). At its top, seismic data reveal normal faults (Fig. 9) with average offsets of only 12 m which form linear rather than amphitheater-like expressions on the sea floor (Fig. 3A). Due to this characteristic, we consider that they are predominantly tectonically induced faults. However, no slope failures have been reported in the Vestnesa area. This phenomenon might be related to the small offset of the faults that is about 3 times less on average than in the southern part of the FSC.

5.3.3 Contourite sedimentation

2D high-resolution seismic data show typical hemipelagic sedimentation patterns without major thickness variations in the northern part of the FSC (Fig. 4). Sediments deposited before the major slope failure more than 5 Ma ago are nearly horizontal with constant thickness. The southern part is characterized by sediment waves and varying thicknesses of sediment layers downslope (Fig. 8). This pattern indicates that contour currents, enhanced sedimentation and erosion influenced sedimentation only in the southern part of the FSC and varied

over time. This interpretation agrees with studies that explain varying sedimentation rates in the Fram Strait with enhanced erosion and fluvial input along the pathway of the West Spitsbergen Current caused by changing currents during different climate conditions (e.g. Gebhardt et al., 2014). The impact of this process might weaken northward as sedimentation rates should decrease down-current and with greater distance from trough mouth fans on the Svalbard margin. This argument is supported by sedimentation rates during the mid to late Weichselian of up to 105 cm per 1000 ^{14}C years in the Vestnesa area and only 10-44 cm per 1000 ^{14}C years on the Yermak Plateau (Howe et al., 2008). Results from ODP Site 912, which most resembles the FSC, do not give very detailed information about sedimentation rates (~30 cm/1000 years in the last 1 Ma) but support the hypothesis of less sediment deposition in the FSC.

Spatially and temporally variable contourite sedimentation (Fig. 8) causes an uneven shape of the slope in the southern part of the FSC. The resulting vulnerably to over-steepening can be a preconditioning factor for slope failure. The geotechnical characteristics of contourites also lower the factor of safety. Silty sediments have low shear strength and are prone to liquefaction, especially if they over-steepen or are exposed to overburden stress (Laberg & Camerlenghi, 2008). We agree that contourites are in general a preconditioning factor for slope failures, especially in areas with cyclic varying sedimentation rates. In combination with toe erosion by rotational slumps these processes may have triggered slope failures.

Despite its similar tectonic setting, large volumes of sediments in the area between Vestnesa and the termination of the Knipovich Ridge did not fail. High contourite sedimentation rates led to the formation of thick drift bodies and sediment waves (Fig. 10), e.g. the Vestnesa Ridge drift. Previous studies linked high sedimentation rates to the generation of overpressure and over-steepening of the margin which led to the conclusion that the area is inherently unstable (Berndt et al., 2009). This assessment is supported by other studies which suggest that the boundary between plumites and rapidly deposited diamicton at the mouth of paleo ice streams on the Svalbard margin favors slope failures due to over-pressure build-up (Lucchi et al.,

2012). . Comparison with the FSC suggests that the rather even margin of the Vestnesa slope in combination with the 20-30% smaller throw of the faults in the Vestnesa area is not as vulnerable to slope failure. In contrast to sediment gravity flows on continental margins, which seek the deepest path and may produce erosion, contourites in general will deposit an irregular blanket of sediment. They can dip at a higher angle than the underlying strata and lead to over-steepening (Laberg & Camerlenghi, 2008) or can smooth out steep slopes (cf. the Isfjorden Drift in Rebesco et al., 2013), which can result e.g. from faulting (Fig. 3B). In Vestnesa, the rate of smoothing of the tectonically-controlled topography by contourites is greater than in the FSC, where faults appear to be more active and favor greater toe erosion.

An integrated and multi-disciplinary investigation of geophysical and geotechnical data, in situ and from laboratory, could be considered to further analyze the difference between the two slides (cf. Vanneste et al, 2014). 3D-information about the subsurface geometry in Vestnesa and FSC in combination with in situ information about shear strength could be used for slope stability calculation. Especially differences in shear strength and soil composition, which are not available at the moment, might offer valuable clues about the different slope stability. Put in a model, this approach could reveal the reason for the different slope failure histories and test all discussed destabilization processes and scenarios. This approach could reveal soil softening behavior and give insights about the suggested retrogressive failure dynamic. Another possibly relevant relationship could exist between hydrate saturation and pore pressure. Measured in situ, this characteristic could reveal possible differences and could be used to calculate the resulting pore pressure. These models might be able to provide the factor of safety of the Vestnesa area and verify the probability of a future slope failure.

5.4 Potential hazards of the FSC in relation to other slope failures on the eastern glaciated North Atlantic continental margin

The volume of sediment that failed during past slope failures ranges from ~2 to 1200 km³ (Table 1); but most of the failure deposits have a volume of less than 70 km³. The headwalls are in 1020 to 2700 m water depth (Fig. 2A) and there is an upslope migration of the headwalls over time in the southern part of the FSC. Compared to characteristics of other large-scale slope failures on the eastern glaciated margin of the North Atlantic, the history of the FSC is much older (cf. Hjelstuen et al., 2007). The volume of most individual events in the FSC is relatively small (< 70 km^3) except for the event in the late Miocene in the northern part of the FSC (N0 in Table 1). Its volume of ~1200 km^3 is comparable to the Tampen, Trænadjupet, Møre and Bjørnøya slides. Berndt et al. (2009), based on numerical models, showed that slope failures with volumes of >1000 km³ have to be considered for hazard assessment in the Fram Strait, as they may cause maximum wave heights of up to 6 m along the shores of the North Atlantic if they originate in ~800 m water depth or less.

There is the potential for future slope failures within the FSC, but the hazard for tsunamis posed by these slope failures is small considering the relatively small volume and great water depth of slope failures that occurred in the past. In addition, the recurrence time of slope failures seems to be very long. The general trend that recent slides have occurred higher up on the slope indicates that the past headwall depth as the limiting factor for the tsunami hazard might not apply to future events. The similarity of geological factors controlling slope stability in the FSC and further south in the area between Vestnesa and Knipovich Ridge might suggest an increased probability of future slope failure there.

On the other hand, this study indicates a potentially positive impact of contourite sedimentation rates on slope stability. Areas with high sedimentation rates were usually associated with high potential for slope failure since many past slope failures in the eastern North Atlantic are located at the end or down-current of trough mouth fans. The high sedimentation rates cause overpressures and make the slope prone to failure. Comparisons made in this study suggest however, that high sedimentation rates of contourites can smooth seabed topography and might reduce the chance of slope failures.

6. Conclusions

The FSC covers an area of ~5500 km² in 850 to 4200 m water depth. Repeated slope failures occurred in the entire FSC since earlier than 5 Ma and evacuated sediments of up to 1160 km³ volume during individual events. The recurrence frequency and volume of the landslides are different in the northern part from the southern part. In the north, one major landslide occurred in the late Miocene. The southern part experienced more frequent, but smaller, slope failures between the late Miocene and late Pleistocene. Analysis of new geophysical data and their comparison with previously published research do not provide any evidence that differences in seismicity as trigger mechanism play an important role nor do regional processes linked to tectonics, climate and oceanography explain the locally different failure patterns. We conclude that local processes are the crucial factors for slope stability in this region.

We cannot identify a distinct reason for the late Miocene major slope failure of ~1160 km³ in the northern part of the survey area. Repeated slope failures in the southern part were most likely due to a combination of toe erosion and slope shape. The distance between upper and lower slope that is characterized by lower gradient, rather than the precise magnitude of the gradient, influenced retrogressive failures. We suggest that rotational block movement along gravity-driven faults must have destabilized the slope from the bottom and may have led

to retrogressive slope failure. Over-steepening and uneven sediment loading along the slope due to patchy sedimentation favored this process. This slope geometry and the smaller throw of the faults at the toe seem to be the main differences when comparing the FSC to the intersection of the Molløy Transform Fault with the Knipovich Ridge. In the latter area, high contourite sedimentation rates led to the formation of thick drift bodies, e.g. the Vestnesa Ridge drift, and smoothed the tectonically controlled margin shape. We rule out dissociation of gas hydrate due to changes in temperature and pressure conditions as the determining factor for slope destabilization because the area was always within the hydrate stability zone. However, overpressure caused by free gas underneath the BSR may have influenced slope stability in the southern part of the FSC. We suggest a future multidisciplinary investigation that combines geophysical and geotechnical information in a joined model to test the discussed processes. Due to the relatively small volumes of the recent slides (up to 62 km^3) in the southern part of the FSC and the relatively great water depth, the tsunami potential of the FSC seems to be small. Only if future slope failures in the region cut further back onto the Yermak Plateau or mobilize much larger portions of the slope, could the system generate sizeable tsunamis.

Acknowledgements

We thank the captain of R.V. Maria S. Merian and his crew for their excellent support at sea. Ship time for cruise MSM31 was provided by the DFG Senatskomission für Ozeanographie. J.E. was financed by the Helmholtz graduate school HOSST. Cruise related data are available on PANGEA.

References

Berndt, C., Brune, S., Nisbet, E., Zschau, J., Sobolev, S.V., 2009. Tsunami modeling of a submarine landslide in the Fram Strait. Geochemistry, Geophysics, Geosystems 10. Q04009, doi:10.1029/2008GC002292

Berndt, C., Bünz, S., Clayton, T., Mienert, J., Saunders, M., 2004. Seismic character of bottom simulating reflectors: examples from the mid-Norwegian margin. Marine and Petroleum Geology 21, 723-733.

Beszczynska-Möller, A., Fahrbach, E., Schauer, U., Hansen, E., 2012. Variability in Atlantic water temperature and transport at the entrance to the Arctic Ocean, 1997–2010. ICES Journal of Marine Science 69, 852-863.

Bourke, R.H., Weigel, A.M., Paquette, R.G., 1988. The westward turning branch of the West Spitsbergen Current. Journal of Geophysical Research 93, 14065-14077.

Bryn, P., Berg, K., Forsberg, C.F., Solheim, A., Kvalstad, T.J., 2005. Explaining the Storegga Slide. Marine and Petroleum Geology 22, 11-19.

Bünz, S., Polyanov, S., Vadakkepuliyambatta, S., Consolaro, C., Mienert, J., 2012. Active gas venting through hydrate-bearing sediments on the Vestnesa Ridge, offshore W-Svalbard. Marine Geology 332-334, 189-197.

Campbell, D.C., Shimeld, J.W., Mosher, D.C., Piper, D.J.W., 2004. Relationships between sediment mass-failure modes and magnitudes in the evolution of the Scotian Slope, offshore Nova Scotia. Offshore Technology Conference paper 16743, 14 p

Dumke, I., Burwicz, E.B., Berndt, C., Klaeschen, D., Feseker, T., Geissler, W.H., Sarkar, S., 2016. Gas hydrate distribution and hydrocarbon maturation north of the Knipovich Ridge, western Svalbard margin. Journal of Geophysical Research 121, doi: 10.1002/2015JB012083.

Elger, J., Berndt, C., Krastel, S., Piper, D.J.W., Gross, F., Spielhagen, R.F., Meyer, S., 2015. The Fram Slide off Svalbard: a submarine landslide on a low-sedimentation-rate glacial continental margin. Journal of the Geological Society 172, 153-156.

Engen, Ø., Eldholm, O., Bungum, H., 2003. The Arctic plate boundary. Journal of Geophysical Research 108, 2075, doi:10.1029/2002JB001809, B2.

Engen, Ø., Faleide, J.I., Dyreng, T.K., 2008. Opening of the Fram Strait gateway: A review of plate tectonic constraints. Tectonophysics 450, 51-69.

Gardner, J.V., Prior, D.B., Field, M.E., 1999. Humboldt Slide – a large shear-dominated retrogressive slope failure. Marine Geology 154, 323-338.

Gebhardt, A.C., Geissler, W.H., Matthiessen, J., Jokat, W., 2014. Changes in current patterns in the Fram Strait at the Pliocene/Pleistocene boundary. Quaternary Science Reviews 92, 179-189.

Haflidason, H., de Alvaro, M.M., Nygard, A., Sejrup, H.P., Laberg, J.S., 2007. Holocene sedimentary processes in the Andøya Canyon system, north Norway. Marine Geology 246, 86-104.

Haflidason, H., Sejrup, H.P., Nygård, A., Mienert, J., Bryn, P., Lien, R., Forsberg, C.F., Berg, K., Masson, D., 2004. The Storegga Slide: architecture, geometry and slide development. Marine Geology 213, 201-234.

Harding, I.C., Charles, A.J., Marshall, J.E.A., Pälike, H., Roberts, A.P., Wilson, P.A., Jarvis, E., Thorne, R., Morris, E., Moremon, R., Pearce, R.B., Akbari, S., 2011. Sea-level and salinity fluctuations during the Paleocene–Eocene thermal maximum in Arctic Spitsbergen. Earth and Planetary Science Letters 303, 97-107.

Henrich, R., 1998. Dynamics of Atlantic water advection to the Norwegian-Greenland Sea—a time-slice record of carbonate distribution in the last 300 ky. Marine Geology 145, 95-131.

Henrich, R., Baumann, K.-H., 1994. Evolution of the Norwegian Current and the Scandinavian Ice Sheets during the past 2.6 my: evidence from ODP Leg 104 biogenic carbonate and terrigenous records. Palaeogeography, Palaeoclimatology, Palaeoecology 108, 75-94.

Hjelstuen, B.O., Eldholm, O., Faleide, J.I., 2007. Recurrent Pleistocene mega-failures on the SW Barents Sea margin. Earth and Planetary Science Letters 258, 605-618.

Howe, J.A., Shimmield, T.M., Harland, R., 2008. Late quaternary contourites and glaciomarine sedimentation in the Fram Strait. Sedimentology 55, 179-200.

Hühnerbach, V., Masson, D.G., partners of the COSTA-Project, 2004. Landslides in the North Atlantic and its adjacent seas: an analysis of their morphology, setting and behavior. Marine Geology 213, 343-362.

Hunter, J.R., Church, J.A., White, N.J., Zhang, X., 2013. Towards a global regionally varying allowance for sea-level rise. Ocean Engineering 71, 17-27.

Hustoft, S., Bünz, S., Mienert, J., Chand, S., 2009. Gas hydrate reservoir and active methane-venting province in sediments on < 20 Ma young oceanic crust in the Fram Strait, offshore NW-Svalbard. Earth and Planetary Science Letters 284, 12-24.

Ingólfsson, Ó., Landvik, J.Y., 2013. The Svalbard–Barents Sea ice-sheet–Historical, current and future perspectives. Quaternary Science Reviews 64, 33-60.

Kretschmer, K., Biastoch, A., Rüpke, L., Burwicz, E., 2015. Modeling the fate of methane hydrates under global warming. Global Biogeochemical Cycles 29, 610-625.

Karstens, J., Berndt, C., 2015. Seismic chimneys in the Southern Viking Graben – Implications for palaeo fluid migration and overpressure evolution. Earth and Planetary Science Letters 412, 88-100.

Kvalstad, T.J., Andresen, L., Forsberg, C.F., Berg, K., Bryn, P., Wangen, M., 2005. The Storegga slide: evaluation of triggering sources and slide mechanics. Marine and Petroleum Geology 22, 245-256.

Laberg, J.S., Camerlenghi, A., 2008. The significance of contourites for submarine slope stability. In: Rebesco, M., Camerlenghi, A. (Eds.), Contourites. Developments in Sedimentology, 60. Elsevier, Amsterdam, 537–556.

Laberg, J.S., Vorren, T.O., 2000. The Trænadjupet Slide, offshore Norway—morphology, evacuation and triggering mechanisms. Marine Geology 171, 95-114.

Leynaud, D., Mienert, J., Vanneste, M., 2009. Submarine mass movements on glaciated and non-glaciated European continental margins: a review of triggering mechanisms and preconditions to failure. Marine and Petroleum Geology 26, 618-632.

Lindberg, B., Laberg, J.S., Vorren, T.O., 2004. The Nyk Slide—morphology, progression, and age of a partly buried submarine slide offshore northern Norway. Marine Geology 213, 277-289.

Løseth, H., Gading, M., Wensaas, L., 2009. Hydrocarbon leakage interpreted on seismic data. Marine and Petroleum Geology 26, 1304 - 1319.

Lucchi, R.G., Pedrosa, M.T., Camerlenghi, A., Urgeles, R., De Mol, B., Rebesco, M., 2012. Recent submarine landslides on the continental slope of Storfjorden and Kveithola Trough-Mouth Fans (northwest Barents Sea). In: Yamada, Y., Kawamura, K., Ikehara, K., Ogawa, Y., Urgeles, R., Mosher, D., Chaytor, J., Strasser, M. (Eds.), Submarine Mass Movements and Their Consequences. Advances in Natural and Technological Hazards Research 31. Springer, Dordrecht, pp. 735-745.

Manley, T.O., 1995. Branching of Atlantic Water within the Greenland-Spitsbergen Passage: An estimate of recirculation. Journal of Geophysical Research 100, 20627-20634.

Mattingsdal, R., Knies, J., Andreassen, K., Fabian, K., Husum, K., Grøsfjeld, K., de Schepper, S., 2014. A new 6 Myr stratigraphic framework for the Atlantic-Arctic Gateway. Quaternary Science Reviews 92, 170-178.

Mienert, J., Vanneste, M., Bünz, S., Andreassen, K., Haflidason, H., Sejrup, H.P., 2005. Ocean warming and gas hydrate stability on the mid-Norwegian margin at the Storegga Slide. Marine and Petroleum Geology 22, 233-244.

Mosher, D.C., Piper, D.J.W., Campbell, D.C., Jenner, K.A., 2004. Near-surface geology and sediment-failure geohazards of the central Scotian Slope. The American Association of Petroleum Geologists Bulletin 88, 703-723.

Petersen, C.J., Bünz, S., Hustoft, S., Mienert, J., Klaeschen, D., 2010. High-resolution P-Cable 3D seismic imaging of gas chimney structures in gas hydrated sediments of an Arctic sediment drift. Marine and Petroleum Geology 27, 1981-1994.

Piper, D.J.W., Deptuck, M.E., Mosher, D.C., Clarke, J.E.H., Migeon, S., 2012. Erosional and depositional features of glacial meltwater discharges on the eastern Canadian continental margin, in: Prather, B. (Eds.), Deptuck, D., Mohrig, D., van Hoorn, B., Wynn, R., Application of the Principles of Seismic Geomorphology to Continental Slope and Base-of-slope Systems: Case Studies from Seafloor and Near-Seafloor Analogues. SEPM Special Publication, 99, 61-80.

Plaza-Faverola, A., Bünz, S., Johnson, J.E., Chand, S., Knies, J., Mienert, J., Franek, P., 2015. Role of tectonic stress in seepage evolution along the gas hydrate-charged Vestnesa Ridge, Fram Strait. Geophysical Research Letters 42, 733-742.

Quadfasel, D., Gascard, J.-C., Koltermann, K.-P., 1987. Large-scale oceanography in Fram Strait during the 1984 Marginal Ice Zone Experiment. Journal of Geophysical Research 92, 6719-6728.

Rebesco, M., Wåhlin, A., Laberg, J.S., Schauer, U., Beszczynska-Möller, A., Lucchi, R.G., Noormets, R., Accettella, D., Zarayskaya, Y., Diviacco, P., 2013. Quaternary contourite drifts of the Western Spitsbergen marin, Dee-Sea Research 79, 156-168.

Reches, Z., 1987. Mechanical aspects of pull-apart basins and push-up swells with applications to the Dead Sea transform. Tectonophysics, 141, 75-88.

Rudels, B., Fahrbach, E., Meincke, J., Budéus, G., Eriksson, P., 2002. The East Greenland Current and its contribution to the Denmark Strait overflow. ICES Journal of Marine Science 59, 1133-1154.

Sarkar, S., Berndt, C., Minshull, T.A., Westbrook, G.K., Klaeschen, D., Masson, D.G., Chabert, A., Thatcher, K.E., 2012. Seismic evidence for shallow gas-escape features associated with a retreating gas hydrate zone offshore west Svalbard. Journal of Geophysical Research 117, B09102. doi:10.1029/2011JB009126.

Schauer, U., Fahrbach, E., Osterhus, S., Rohardt, G., 2004. Arctic warming through the Fram Strait: Oceanic heat transport from 3 years of measurements. Journal of Geophysical Research 109, C06026. doi:10.1029/2003JC001823.

Schwab, W.C., Danforth, W.W., Scanlon, K.M., Masson, D.G., 1991. A giant submarine slope failure on the northern insular slope of Puerto Rico. Marine Geology 96, 237-246.

Shedd, W., Godfriaux, P., Frye, M., Bowell, R., Hutchinsons, D., 2009. Occurrence and variety in seismic expression of the base of gas hydrate stability in the Gulf of Mexico, USA. DOE-NETL Fire in the Ice Newsletter, Winter 2009, 11-14.

Stigall, J., Dugan, B., 2010. Overpressure and earthquake initiated slope failures in the Ursa region, northern Gulf of Mexico. Journal of Geophysical Research 115, B04101. Doi:10.1029/2009JB006848.

Stocker, T.F., Qin, D., Plattner, G.-K., Tignor, M.M.B., Allen, S.K., Boschung, J., Nauels, A., Xia, Y., Bex, V., Midgley, P.M., 2013. The Physical Science Basis Working Group I Contribution to the Fifth Assessment Report of the Intergovernmental Panel on Climate Change. Cambridge University Press: Cambridge, UK and New York, NY.

Sultan, N., Cochonat, P., Foucher, J.-P., Mienert, J., 2004. Effect of gas hydrates melting on seafloor slope instability. Marine Geology 213, 379-401.

Talwani, M., Eldholm, O., 1977. Evolution of the Norwegian-Greenland Sea. Geological Society of America Bulletin 88, 969-999.

Thiede, J., Myhre, A.M., Firth, J.V. & Shipboard Scientific Party, 1995. Cenozoic Northern Hemisphere Polar and Subpolar Ocean Paleoenvironments (Summary of ODP Leg 151 Drilling Results), in: Myhre, A.M., Thiede, J., Firth, J.V., et al. (Eds.) Proceedings of the Ocean Drilling Program, Initial Reports, US College Station, Texas, 151, pp. 397–420.

Vanneste, M., Guidard, S., Mienert, J., 2005. Bottom-simulating reflections and geothermal gradients across the western Svalbard margin. Terra Nova 17, 510-516.

Vanneste, M., Mienert, J., Bünz, S., 2006. The Hinlopen Slide: A giant, submarine slope failure on the northern Svalbard margin, Arctic Ocean. Earth and Planetary Science Letters 245, 373 - 388.

Vanneste, M., Sultan, N., Garziglia, S., Forsberg, C.F., L'Heureux, J.-S., 2014. Seafloor instabilities and sediment deformation processes: The need for integrated, multi-disciplinary investigations. Marine Geology 352, 183-214.

Winkelmann, D., Stein, R., 2007. Triggering of the Hinlopen/Yermak Megaslide in relation to paleoceanography and climate history of the continental margin north of Spitsbergen. Geochemistry, Geophysics, Geosystems 8, Q06018. doi:10.1029/2006GC001485.

Winkler, A., Wolf-Welling, T., Stattegger, K., Thiede, J., 2002. Clay mineral sedimentation in high northern latitude deep-sea basins since the Middle Miocene (ODP Leg 151, NAAG). International Journal of Earth Sciences 91, 133-148.

Wolf, T.C.W., Thiede, J., 1991. History of terrigenous sedimentation during the past 10 My in the North Atlantic (ODP Legs 104 and 105 and DSDP Leg 81). Marine Geology 101, 83-102.

Zachos, J., Pagani, M., Sloan, L., Thomas, E., Billups, K., 2001. Trends, Rhythms, and Aberrations in Global Climate 65 Ma to Present. Science 292, 686-693.

Table 1: Identified slope failures in the FSC with their minimal estimated age of origin based on the extrapolation of the seismic stratigraphy of Mattingsdal et al. (2014), height and water depth of the head or sidewalls and the estimated evacuated volume.

mass failure	age [Ma]	height [m]	volume [km³]	water depth [m]
S0	>5	60	20.4	1820
N0	>5	600-300	1161.1	1020
S1	5	60-23	37.6	1820
S2	2,58	15	5.2	1650
S3	2,58	53	19.4	1660
S4	1.95-2.58	30	10.3	1750
N1	1.95-2.58	105	13.1	1500
N2	1.2-1.78	38	1.7	1350
S5	1.2	98	32.8	1660
S6	0.78	120	62.3	1290
N3	0.78	23	1.7	1380
S7	0,68	23	3.3	1650
S8	<0.78	180	26.6	1640
SQ1	-	120	23.8	2550
SQ2	-	98	17.1	2470
SQ3	-	90	19.5	2240
NQ1	-	90	13.4	1670

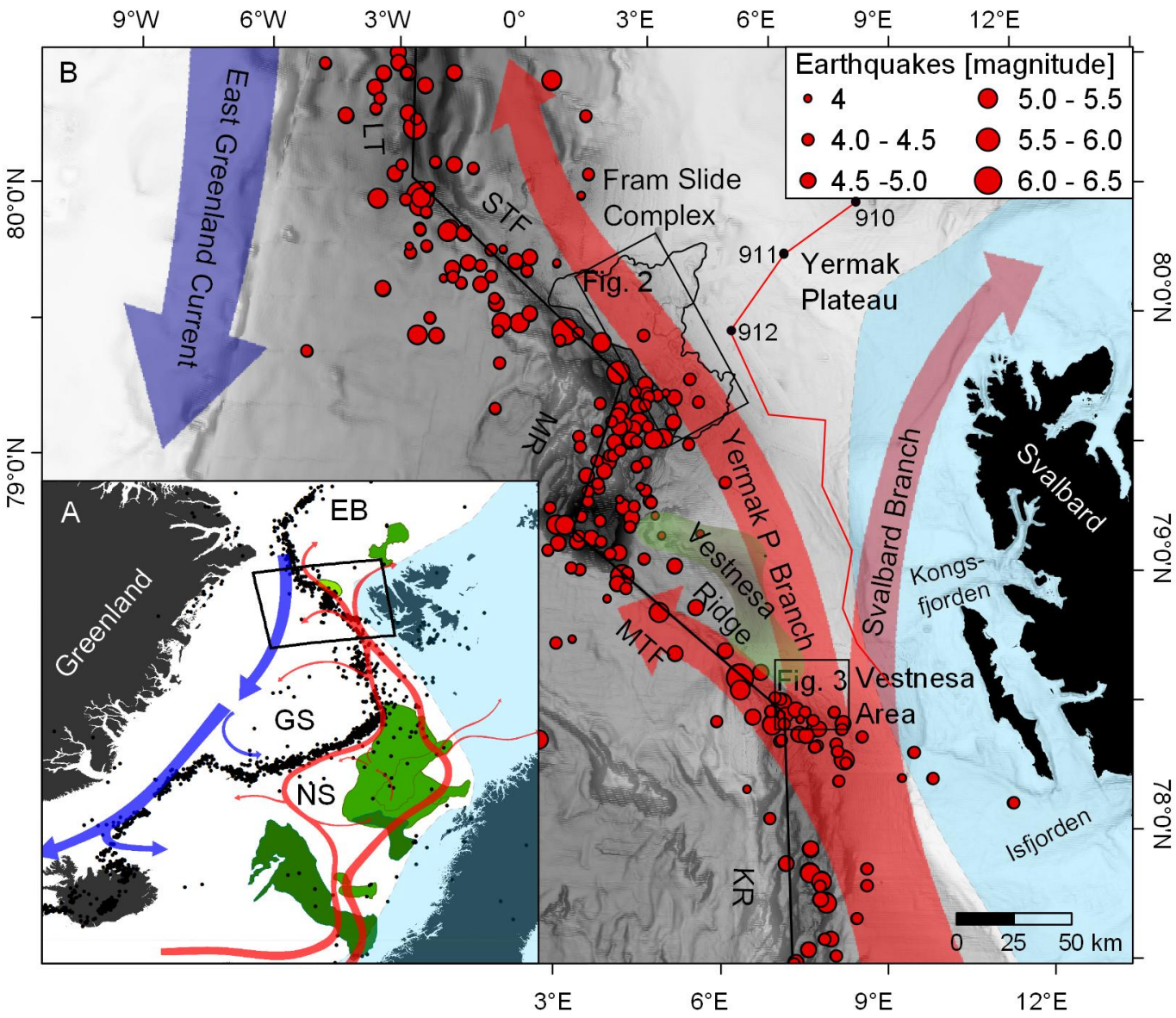

Fig. 1: Location of the Fram Slide Complex on the continental margin off Svalbard: (A) overview map with the location of the Norwegian and Greenland Sea (NS and GS), the Eurasian Basin (EB), the surface water circulation in the eastern North Atlantic including the East Greenland Current and the West Spitsbergen Current (red arrows) (adapted from Beszczynska-Möller et al., 2012), the sea floor affected by the Holocene Andøya, Trænadjupet and Storegga slides (light green, north to south), and by the Pleistocene Hinlopen–Yermak, Vigid, Sklinnadjupet, Bjørnøya Fan Slide Complex and Bjørnøya slides (dark green, north to south) (Haflidason et al., 2007; Winkelmann and Stein, 2007) and the location of the FSC (outlined in black) (map projection: azimuthal equidistant). (B) Regional bathymetry of the Fram Strait and Svalbard margin with the Lena Trough (LT), the

Spitsbergen Transfer Fault (STF), Molløy Ridge (MR), Molløy Transfer Fault (MTF) and Knipovich Ridge (KR), the location of the ODP bore holes 910-912, the seismic profiles from which the stratigraphy of Mattingsdal et al. (2014) was extrapolated, the branches of the splitting West Spitsbergen Current, the northern and southern part of the FSC (NP and SP) and the location of Figs. 2 and 3 (map projection: WGS 1984 UTM Zone 32N). Both maps show the maximum ice extent during glacial periods since 100 ka (blue shapes) (adapted from Ingólfsson and Landvik, 2013) and seismicity in the area between 1973 and 2015 (M >4) (black and red dots in (A) and (B), respectively; source: US Geological Survey).

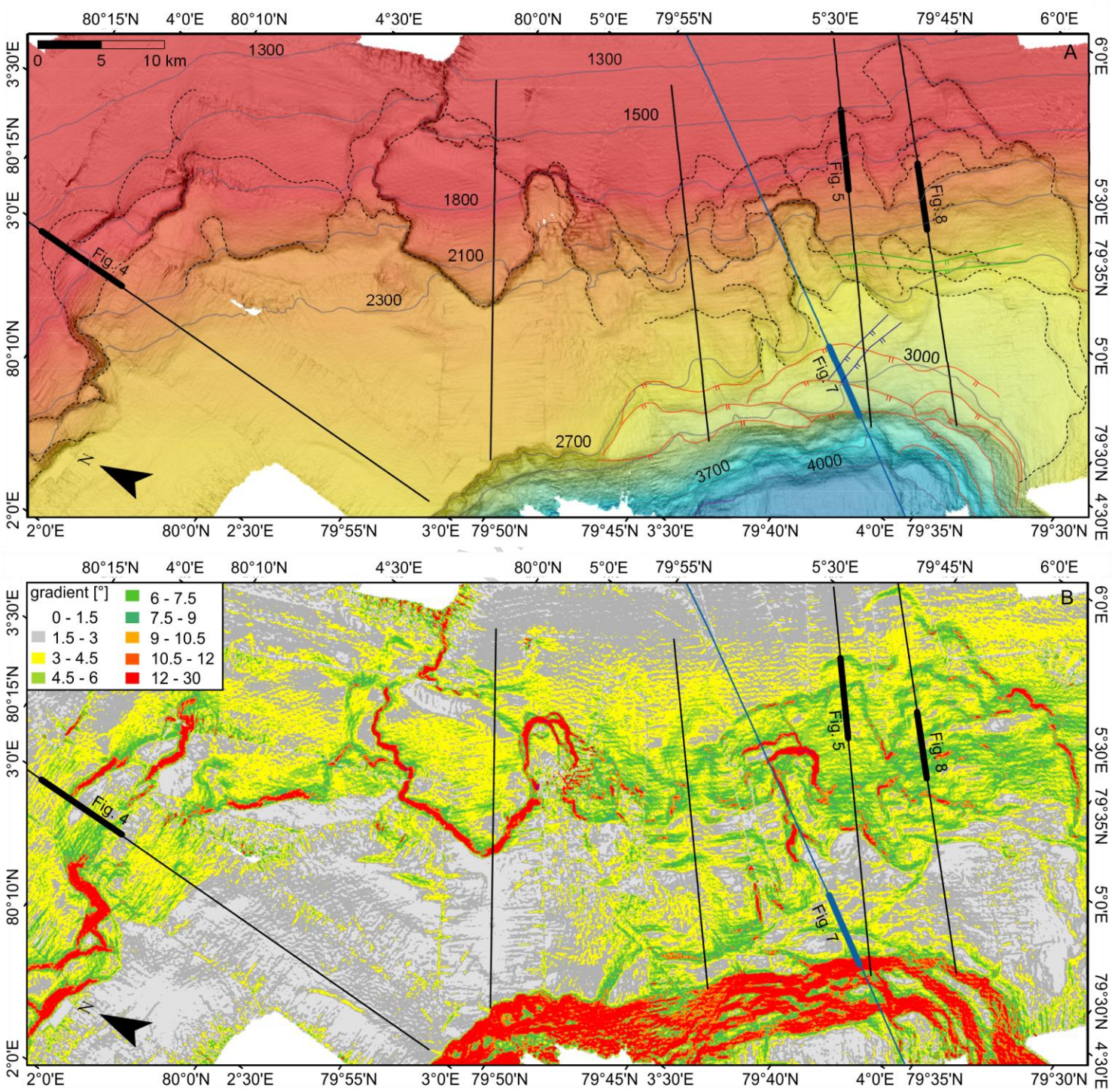

Fig. 2: Maps (map projection: WGS 1984 UTM Zone 32N) of the FSC of (A) local bathymetric data with contour lines (gray lines in meters), head- and sidewalls (black dashed lines) and normal curved faults that trace the shape of the deep water pathway (red lines), faults with a strike direction of ~55° dip towards the southwest (green line) and faults that strikes ~10° and dips south-southwest (blue lines); (B) slope gradient of the FSC.

Both maps show the reflection seismic profiles from MSM31 (black lines) and MSM21-4 (blue line) and the location of Figs. 4, 5, 7 and 8 (bold lines).

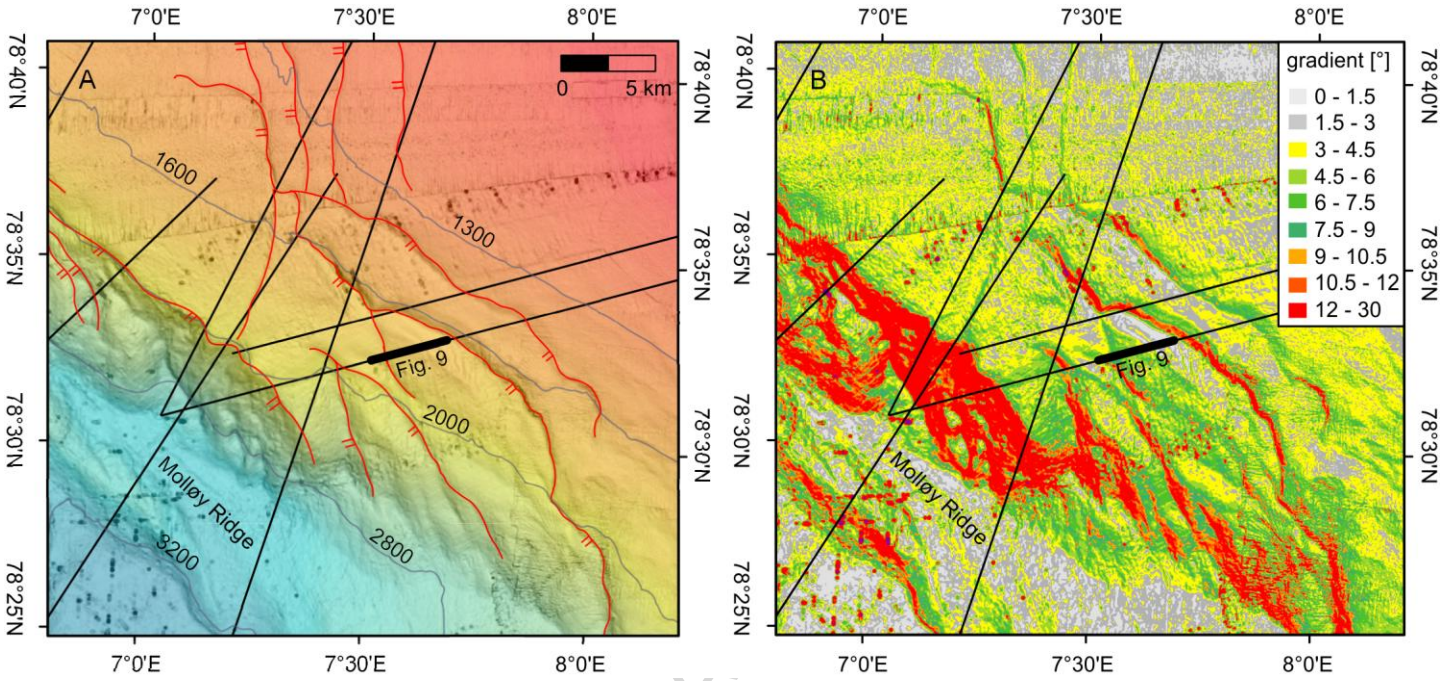

Fig. 3: Maps (projection: WGS 1984 UTM Zone 32N) of the Vestnesa area of (A) local bathymetric data with contour lines (gray lines in meters) and normal faults (red lines); (B) slope gradient. The reflection seismic profiles from MSM 21-4 and the location of Fig. 9 are indicated by black and bold black lines, respectively.

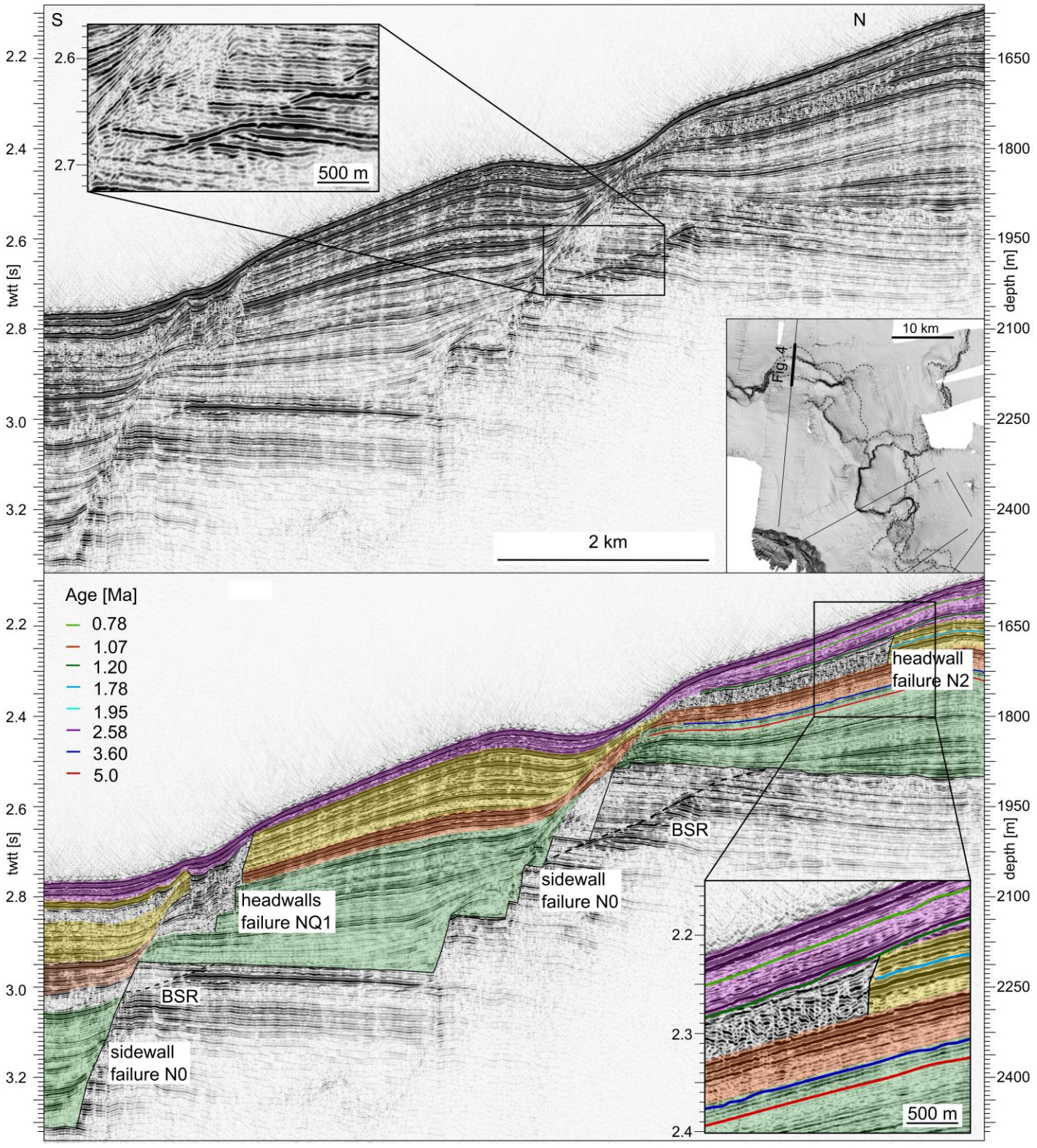

Fig. 4: An extract of the reflection seismic profile MSM31-P385 (top) with a zoom to truncated well-stratified sediments in the northern part of the FSC and its interpretation (bottom) showing the major ancient sidewall of

the slope failure N0, the BSR (dashed line) visible in the pre failure sediments, more recent failures (N2 and NQ1) in the vicinity of the old sidewall and the extrapolated stratigraphy from Mattingsdal et al. (2014) (colored lines) that we used to estimate the age. The colored intervals of reflections indicate characteristic sediment units with distinctive architecture.

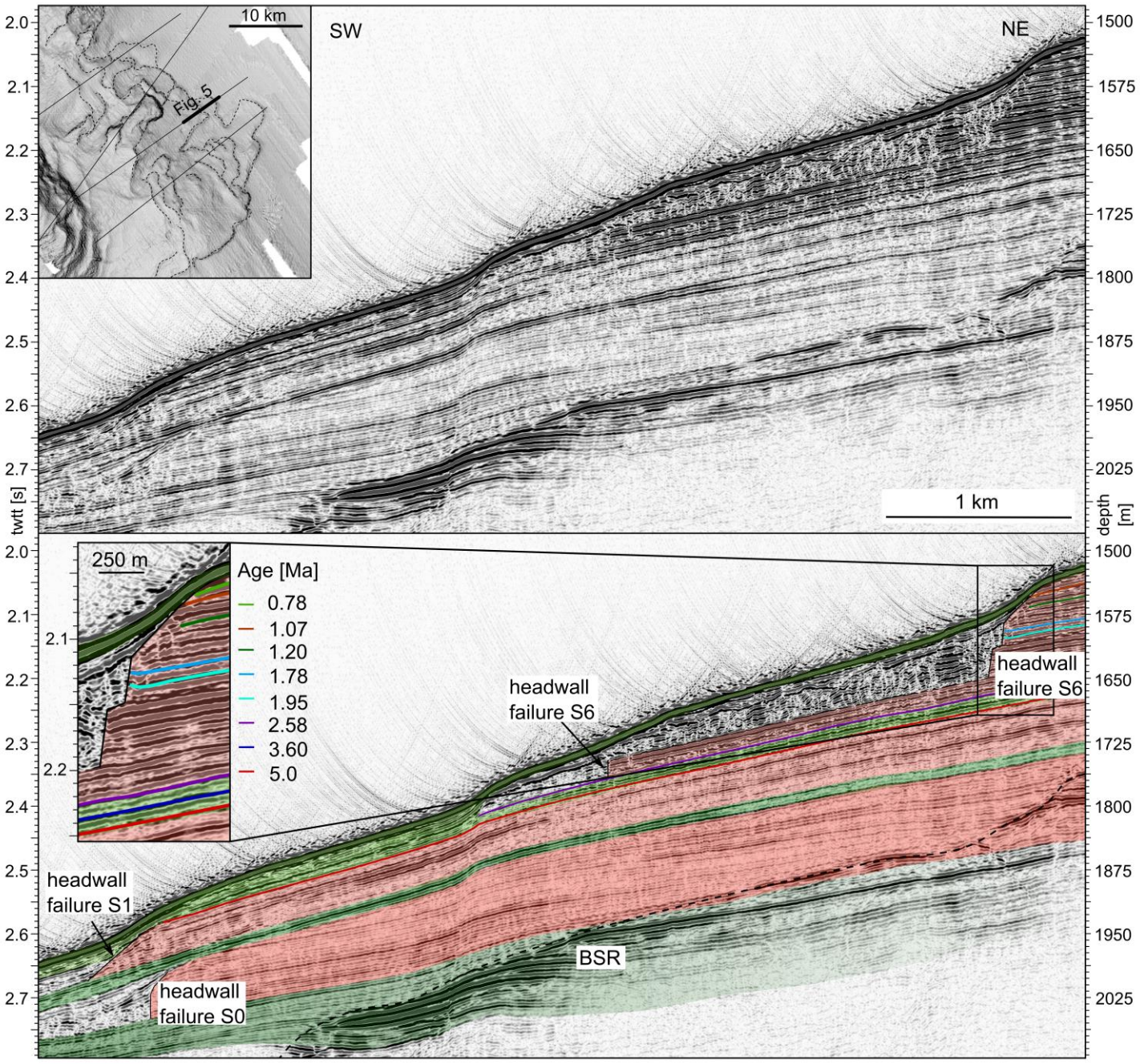

Fig. 5: An extract of the reflection seismic profile MSM31-P370 (top) in the southern part of the FSC and its interpretation (bottom) showing the buried headwalls of multiple failures (S0, S1 and S6), a continuous BSR (dashed line) in ~300 ms twtt parallel to the sea floor reflection and a detailed zoom to the headwall of the slope failure S6 with the seismic stratigraphy adapted from Mattingsdal et al. (2014). The colored intervals of reflections indicate characteristic sediment units with distinctive architecture.

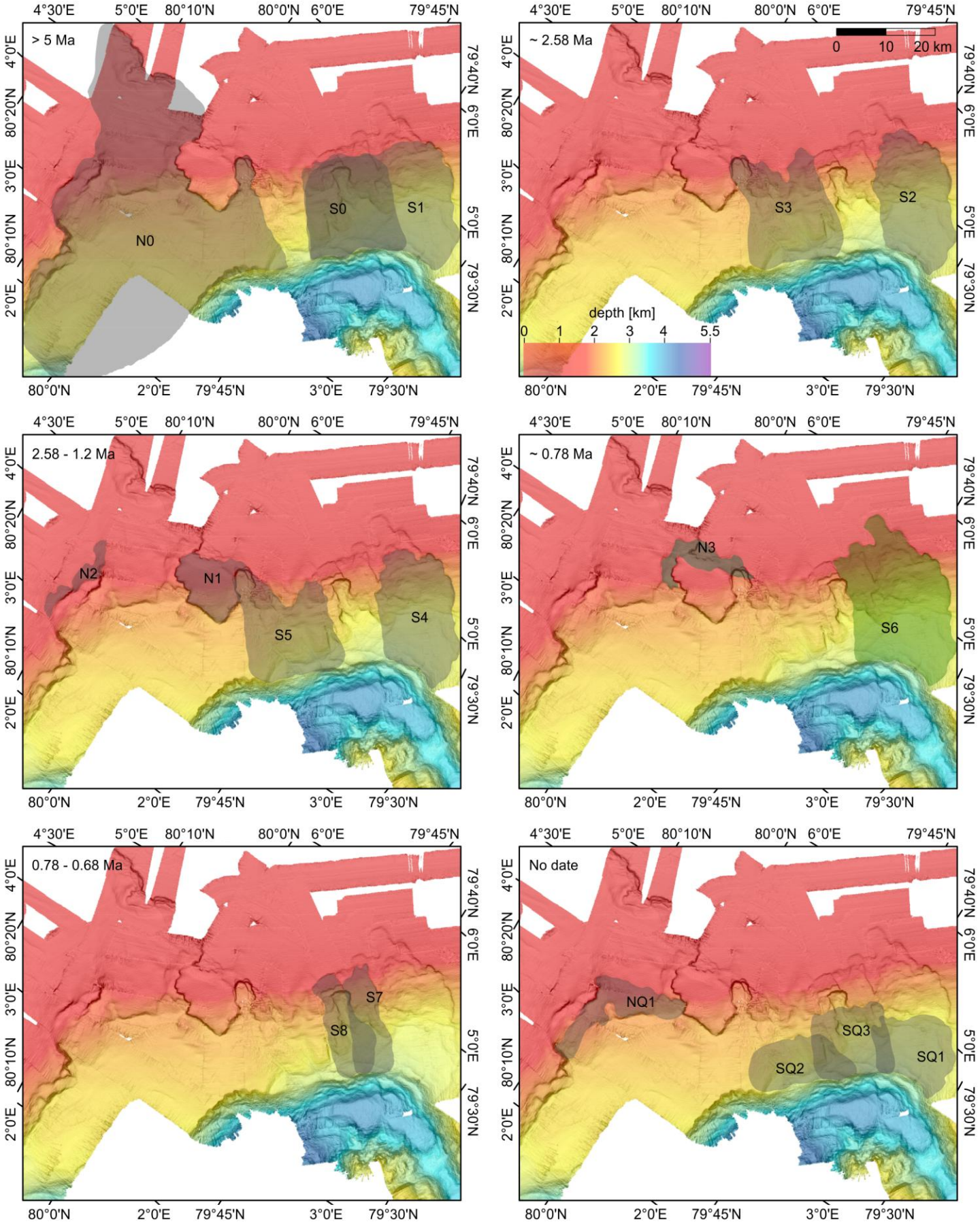

Fig. 6: Bathymetric maps with the history of slope failures of the FSC. Five bathymetric maps represent time intervals from more than 5 Ma ago until 0.68 Ma before present. They show the areas (in grey) influenced by the slope failures listed in Table 1. Age estimates are based on the extrapolation of the seismic stratigraphy of Mattingsdal et al. (2014). An additional map shows the slope failures with no age estimate.

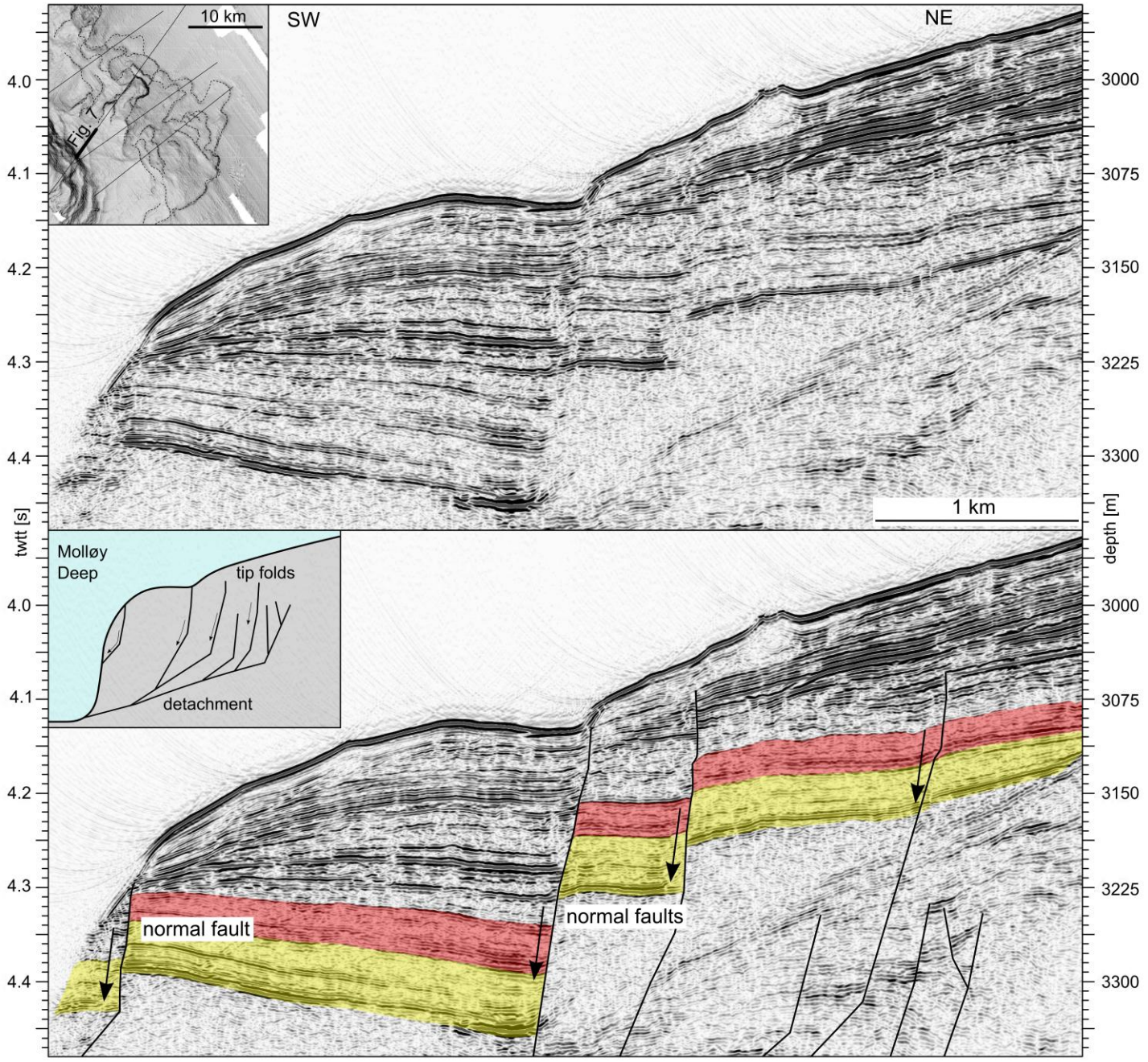

Fig. 7: An extract of the reflection seismic profile MSM21_4-P500 (top) in the southern part of the FSC and its interpretation (bottom) showing normal faults in ~3 km water depth with different offset and of different age and a line draw of the lower slope in the southern part of the FSC next to the Molløy Deep. The colored groups of reflections indicate characteristic sediment units.

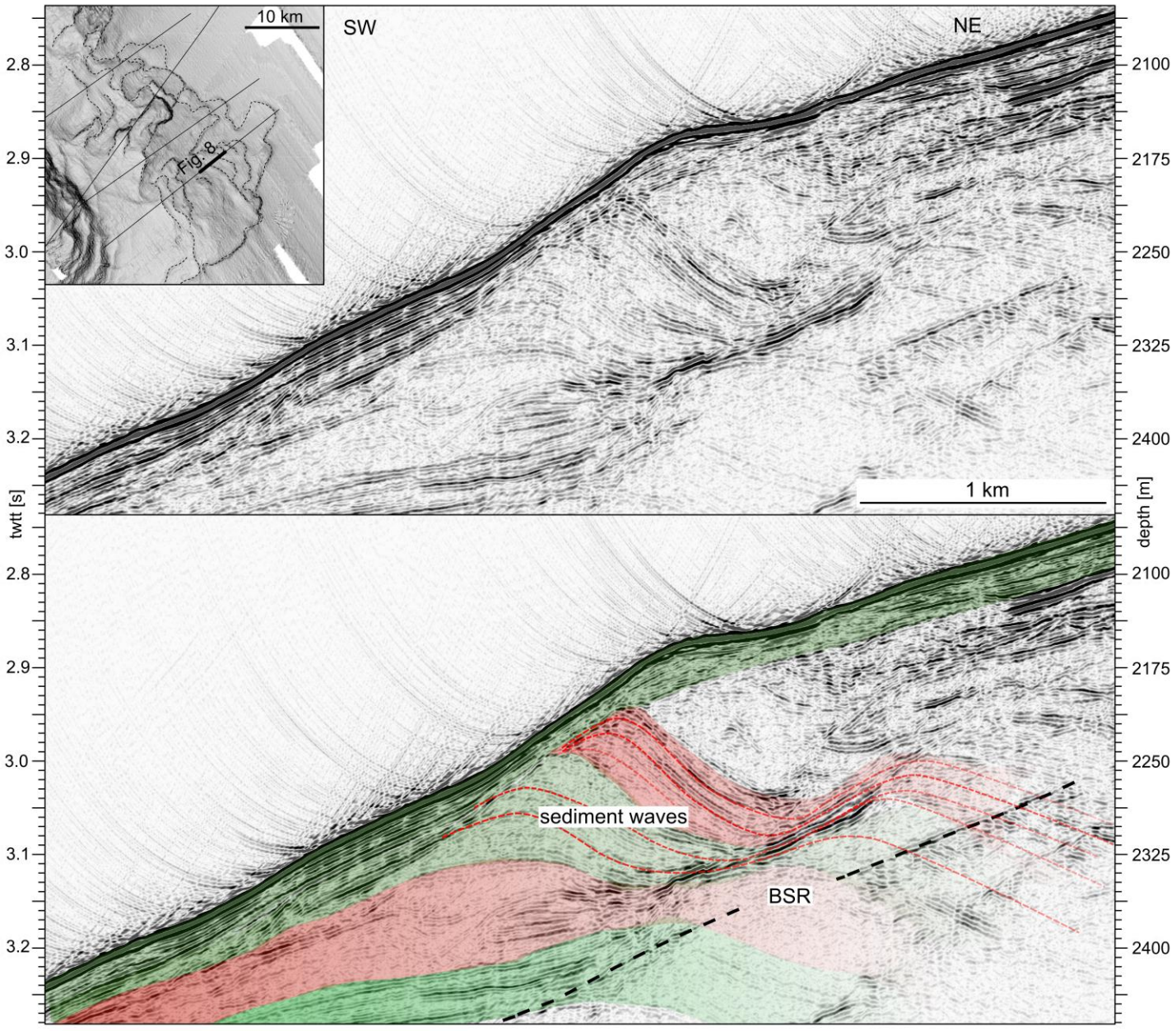

Fig. 8: An extract of the reflection seismic profile MSM31-P365 (top) in the southern part of the FSC and its interpretation (bottom) showing sediments waves (dashed red line) and a patchy BSR (dashed black line). The colored groups of reflections indicate characteristic sediment units, not stratigraphic layers.

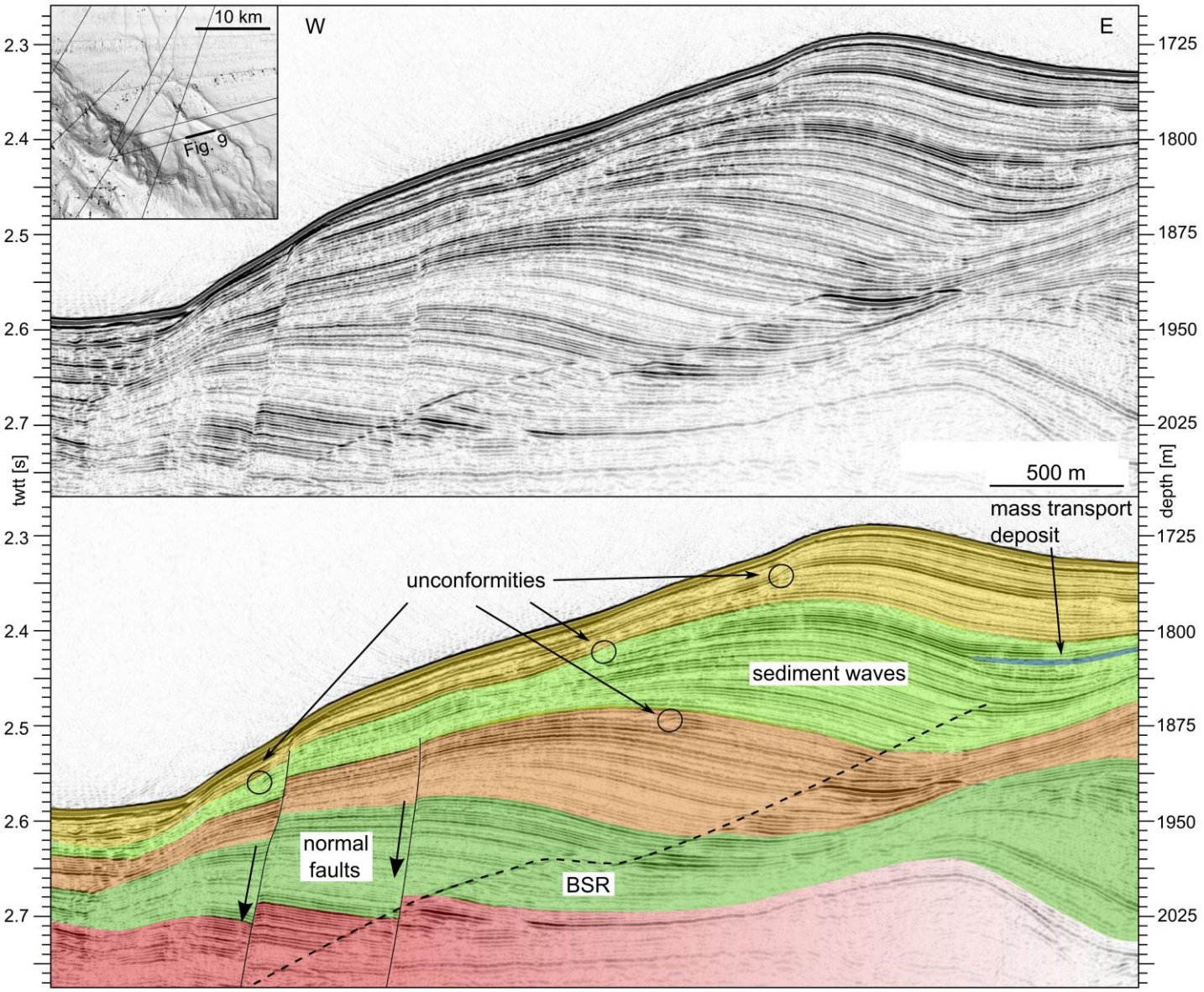

Fig. 9: An extract of the reflection seismic profile MSM21_4-P100 (top) in Vestnesa area and its interpretation (bottom) showing sediments waves, the BSR (dashed black line), normal faults, unconformities and small mass transport deposits. The colored groups of reflections indicate characteristic sediment units.

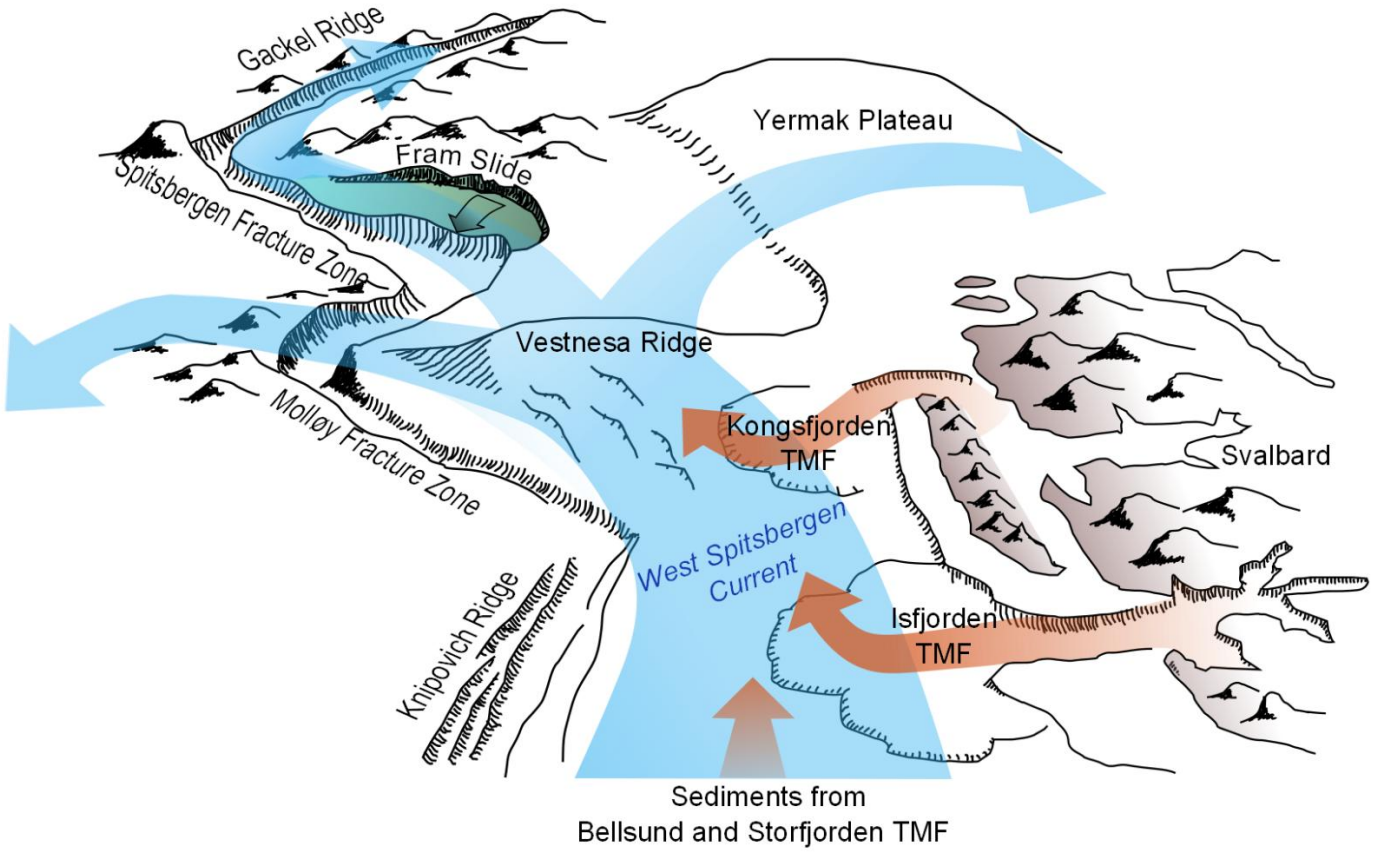

Fig. 10: Schematic diagram of the Fram Strait region showing the main current patterns and sediment sources with respect to the tectonic elements. The West Spitsbergen Current (blue arrow) transports the sediment (orange arrows) from the main ice streams northwards. Sedimentation rates are highest at Vestnesa Ridge where the West Spitsbergen Current splits into different branches. While all other factors (climate, sea level change, seismicity, sedimentary fluid migration systems, and sediment type) are similar we infer that it is the smoothing of topography in this high sedimentation environment that prevents toe erosion and undercutting of steep slopes that might lead to slope failures on Vestnesa Ridge. Farther north in the region of the Fram Slide steep morphology due to tectonic forces and previous slope failures is preserved much longer and makes it susceptible to further mass wasting.